2011 50th IEEE Conference on Decision and Control and
European Control Conference (CDC-ECC)
Orlando, FL, USA, December 12-15, 2011

# Flutter Control of Long-Span Suspension Bridges

Xiaowei Zhao, David J. N. Limebeer and J. Michael R. Graham

*Abstract*— **The dynamic stabilization of a sectional model of a long-span suspension bridge is considered. Feedback control is achieved using leading- and trailing-edge flaps as actuators. While a wide variety of control systems is possible, we focus on compensation schemes that can be implemented using passive mechanical components such as springs, dampers, and a rack and pinion mechanism. A single-loop control system is investigated that controls the flaps by sensing the main deck heave velocity. A symmetrical control scheme is used on both flaps to make the feedback system insensitive to the wind direction. The key finding is that the critical wind speed for the flutter instability of the sectional model of the bridge can be greatly increased, with good robustness characteristics, through passive feedback control.**

## I. Introduction

The now iconic Tacoma Narrows bridge disaster (1940) was caused by the gradual growth, over a period of approximately 45 minutes, of a torsional flutter oscillation. It was subsequently established that the Tacoma Narrows bridge failure resulted from the use of a structurally and aerodynamically inappropriate squat H-section structure for the main bridge deck [1]. One possible modification to the aeroelastic properties of the bridge structures is to introduce stationary, or actively controlled aerodynamic flutter suppression surfaces. In [2] we present a 2D aerodynamic model of a long-span suspension bridge with controllable leading- and trailing-edge flaps; see Fig. 1. In this work we make use of the thin aerofoil theory first developed by Theodorsen [3] to study flutter - this theory also exposes a non-oscillatory instability known as torsional divergence. The torsional divergence mode is a bona fide aeroelastic mode that goes unstable when there is a loss of torsional rigidity due to the cancelation of the (positive) torsional stiffness of the structure by the negative pitch-related aerodynamic moment.

This paper investigates the utility of a symmetric (with respect to wind direction) aerodynamic control system that will be evaluated by numerical simulation. There are supplementary issues to consider that relate to control surface flow separation and compromised actuator effectiveness due to their immersion in the main deck's wake.

A lot of good work has been done on the aerodynamic control of cable-stayed suspension bridges. This literature falls into four broad categories, and while much progress has been made, each approach has its short-comings. Passive pure-gain controllers [4], [5] are in principle easy to implement, but these systems forego the advantages that might accrue from some form of phase compensation. Fixed-phase controllers, such as those described in [6], are not physically realizable. Realizable systems that introduce frequency-dependent phase compensation may operate satisfactorily, but this has not thus far been established. Active controllers, such as those based on linear optimal control and $\mathcal{H}^\infty$ [7], face severe reliability questions, because they are relatively complicated and will require a power supply and probably also a computer system. Bad weather situations may well result simultaneously in high winds and power supply failures. Adaptive controllers, such as variable gain output feedback controllers [8], face the same difficulties. Our purpose is to address some of these issues and contribute to the better understanding of these systems. It is a truism that computer models can be useful, but they are never 'right'. As a result, one must be mindful of robust stability and robust performance issues [9], because ultimately it is the bridge and not the bridge model that must be stabilized. Robustness is an important issue that appears not to have been considered in the long-span bridge design context.

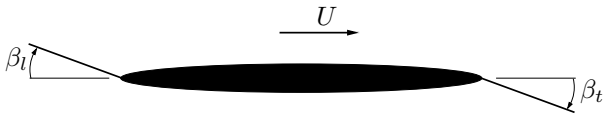


Fig. 1. Cross section of a long-span suspension bridge with controllable flaps. The wind speed is denoted $U$, while the leading- and trailing-edge flap angles are denoted $\beta_l$ and $\beta_t$ respectively.

## II. Dynamic Model

We begin by describing the structural and aerodynamic models of the bridge section with leading- and trailing-edge controllable flaps developed in [10], [2]. Referring to the diagram of the system kinematics in Fig. 2, we see that the generalized coordinates are the deck's heave $h$ and pitch angle $\alpha$, and the flap angles $\beta_t$ and $\beta_l$.

The heave and pitch dynamics are described by:

$$M_h\ddot{h} + 2\omega_h\zeta_h\dot{h} + K_h h = L, \tag{1}$$

$$J_p\ddot{\alpha} + 2\omega_p\zeta_p\dot{\alpha} + K_p\alpha = M, \tag{2}$$

where $L$ is the aerodynamic lift force; $M$ is the aerodynamic moment around $O$ as shown in Fig. 2; $M_h$ and $J_p$ are the mass and the torsional mass moment of inertia, per unit length, respectively; $\omega_h$ and $\omega_p$ are the undamped natural frequencies of the heave mode and pitch mode; $\zeta_h$ and $\zeta_p$

This work was funded by the UK EPSRC.

X. Zhao and D. J. N. Limebeer are with the Department of Engineering Science, University of Oxford, Parks Road, Oxford OX1 3PJ, United Kingdom, e-mail: xiaowei.zhao@eng.ox.ac.uk, david.limebeer@eng.ox.ac.uk

J. M. R. Graham is with the Department of Aeronautical Engineering, Imperial College London, London SW7 2AZ, United Kingdom, e-mail: m.graham@imperial.ac.uk

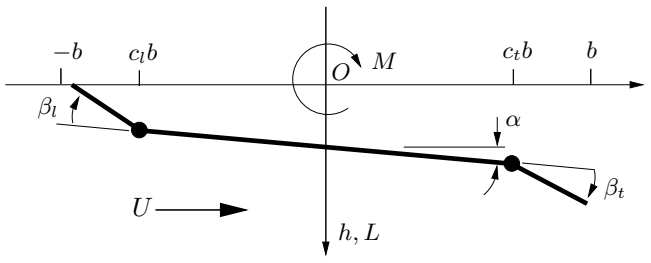


Fig. 2. Kinematic model of the bridge deck. The origin of the inertial axis system is $O$. The wind velocity $U$ is assumed positive to the right, the heave $h$ and lift force $L$ are assumed to be positive downwards, moments $M$ are positive clockwise, as are the pitch and flap angles $\alpha$, and $\beta_l$ and $\beta_t$ respectively. The deck chord (including the flaps) is $2b$. The leading- and trailing-edge flap chords are $(1+c_l)b$ and $(1-c_t)b$ respectively; note that $c_l < 0$.

are the structural damping coefficients; $K_h = M_h\omega_h^2$ and $K_p = J_p\omega_p^2$ are the per unit length heave and torsinal deck stiffness respectively.

The aerodynamic model is based on unsteady thin aerofoil theory as was described in the first instance by [3]. The lift and moment on the system are given by

$$L = \rho b^3\omega^2\left\{L_h\frac{h}{b} + L_\alpha\alpha + L_{\beta_t}\beta_t + L_{\beta_l}\beta_l\right\}, \quad (3)$$

$$M = \rho b^4\omega^2\left\{M_h\frac{h}{b} + M_\alpha\alpha + M_{\beta_t}\beta_t + M_{\beta_l}\beta_l\right\} \quad (4)$$

in which $b$ and $\rho$ are the half chord of the deck and the air density respectively. The aerodynamic derivatives $L_h$, $L_\alpha$, $L_{\beta_t}$, $M_h$, $M_\alpha$ and $M_{\beta_t}$ corresponding to the various perturbation variables, can be derived by direct calculation from equation (XVIII) or (XX) in [3]. One may verify that

$$L_{\beta_t}(c_t) = \frac{jT_4(c_t)}{k} - T_1(c_t) - C(k)\left(\frac{2T_{10}(c_t)}{k^2} + \frac{jT_{11}(c_t)}{k}\right)$$

in which $C(k)$ is the Theodorsen function

$$C(k) = \frac{J_1(k) - jY_1(k)}{(J_1(k)+Y_0(k)) - j(J_0(k)-Y_1(k))}, \quad (5)$$

in which $J_0(k)$, $J_1(k)$, $Y_0(k)$ and $Y_1(k)$ are Bessel functions of the first and second kind respectively, $k = \omega b/U$ is the reduced frequency [11] and $j = \sqrt{-1}$. The functions $T_i(\cdot)$ are defined in [3].

The Theodorsen function is an irrational function of the reduced frequency, and it is convenient, for computational reasons, to make use of a rational approximation. Motivated by a desire to study transient (non-steady) phenomena, Jones and Sears introduced operational methods (and the Laplace transform) into aeroelastic theory [12]. Rational approximations of the Theodorsen function and other irrational quantities allow one to replace techniques such as the $k$-method and the $(p-k)$-method with classical control devices such as root locus and Nyquist diagrams. By invoking a linear least squares approximation, the authors found an accurate quartic approximation to the Theodorsen function [10], [2], whose numerator and denominator coefficients are given in Table I. The interested reader can find more on high-fidelity approximations in unsteady flow problems in [13]. Here $\hat{s} = \frac{sb}{U}$ is the reduced Laplace transform variable.

| numerator terms | denominator terms |
|---|---|
| 0.99592 | 1 |
| 57.01896 $\hat{s}$ | 62.30441 $\hat{s}$ |
| 623.78848 $\hat{s}^2$ | 807.78489 $\hat{s}^2$ |
| 1895.46328 $\hat{s}^3$ | 3060.67868 $\hat{s}^3$ |
| 1523.24700 $\hat{s}^4$ | 3033.76379 $\hat{s}^4$ |

TABLE I
NUMERATOR AND DENOMINATOR COEFFICIENTS OF A QUARTIC APPROXIMATION TO THE THEODORSEN FUNCTION.

The aerodynamic derivatives for a leading-edge flap can be derived using superposition methods [10], [2]:

$$L_{\beta_l}(c_l) = L_{\beta_t}(c_l) - L_\alpha - c_l b L_h, \quad (6)$$

$$M_{\beta_l}(c_l) = M_{\beta_t}(c_l) - M_\alpha - c_l b M_h. \quad (7)$$

## III. Feedback Control System

We will now present a control system which uses the bridge deck heave velocity as a feedback signal and the flap angles as control inputs. In the sequel, we will use the Akashi Kaikyo bridge [5] as working example:

$$2b = 30\,m,\ M_h = 33,600\,kg/m,\ J_p = 4.97\times10^6\,kg\,m^2,$$
$$\omega_h = 0.427\,rad/s,\ \omega_p = 0.917\,rad/s,\ \zeta_h = 0.0083,$$
$$\zeta_p = 0.0072 \text{ and } \rho = 1.23\,kg/m^3.$$

For this bridge the critical wind speeds for flutter and torsional divergence are approximately 52 m/s and 70 m/s respectively [4]. While our control scheme cannot influence the critical wind speed for torsional divergence, we aim to increase the critical wind speed for flutter to match that for torsional divergence.

### A. Control System Design and Open-Loop Response

A block diagram of the bridge deck control system with its structural dynamics, fluid dynamics and flap controller is given in Fig. 3. The uncontrolled system is described by the plant $P(s)$ that contains the structural dynamics and the non-circulatory part of the fluid mechanics. A finite-dimensional approximation to the Theodorsen function that generates the circulatory flow is given as $C(s)$. The leading- and trailing-edge flaps have the same flap length and use the same controller $K(s)$, which has the deck heave velocity $\dot{h}(s)$ as input and so single-loop Nyquist diagrams can be plotted by breaking the feedback loop at $\Delta$. This control system is independent to wind direction, but it is ineffective to improving critical wind speed for torsional divergence, because of the offset effect of the flaps on critical torsional divergence speed. In the study presented here the system is represented in terms of a generalized state-space model of the form

$$E\dot{x} = Ax + Bu \quad (8)$$

$$z = Cx, \quad (9)$$

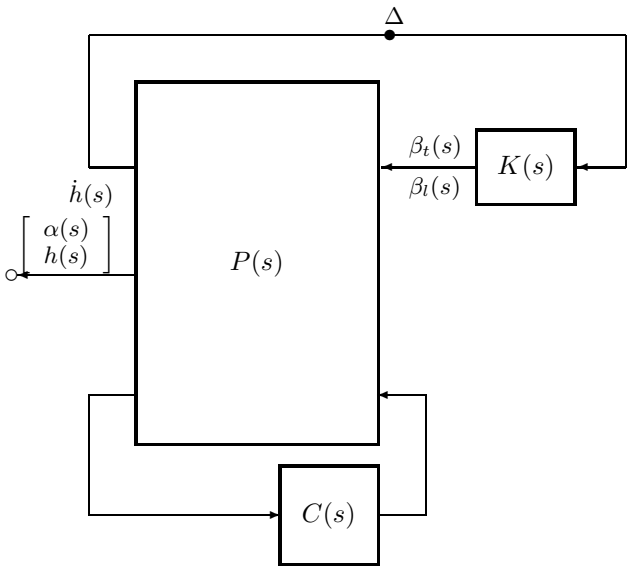


Fig. 3. Block diagram of the flutter control system with heave velocity feedback. The dynamics of the bridge are represented by the plant $P(s)$ and the Theodorsen function $C(s)$; 's' is the Laplace variable. The flaps control system is given by $K(s)$. The leading- and trailing-edge flap angles are given by $\beta_l(s)$ and $\beta_t(s)$, and the deck pitch angle and heave are given by $\alpha(s)$ and $h(s)$ respectively.

which is an assembly of equations (1), (2), (3), (4) and a rational approximation to (5). The control input $u(t) = [\beta_t(t)\ \beta_l(t)]'$ in (8) comprises the leading- and trailing-edge flap angles, while the system output in (9) is $z(t) = \dot{h}(t)$. Figures of this type are standard in the control systems literature with more detail available in [9].

Since the controlled inputs (in the model) are the flap angles rather than torques applied to massy flap bodies, the model given in (8) must generate the first and second derivatives of the flap angles internally; these derivatives are required by the aerodynamic model. This is achieved using a generalized state-space system of the form

$$\begin{bmatrix} 0 & 0 \\ 1 & 0 \end{bmatrix} \begin{bmatrix} \dot{x}_1 \\ \dot{x}_2 \end{bmatrix} = \begin{bmatrix} 1 & 0 \\ 0 & 1 \end{bmatrix} \begin{bmatrix} x_1 \\ x_2 \end{bmatrix} + \begin{bmatrix} -1 \\ 0 \end{bmatrix} \beta, \quad (10)$$

where $\beta$ denotes a flap angle. It follows immediately that

$$x_1 = \beta; \quad x_2 = \dot{\beta} \quad \text{and} \quad \dot{x}_2 = \ddot{\beta},$$

thereby establishing that the required flap-angle derivatives can be constructed in this way. Since (10) has both its eigenvalues at infinity, (8) will have four eigenvalues there. These eigenvalues are not associated with 'real' system dynamics, or system stability properties and are thus ignored for present purposes.

The class of mechanical controllers $K(s)$ we are considering in this papers are illustrated in Figure 4, where the bridge's heave velocity $\dot{h}$ (which is positive downwards) is used to manipulate mechanically the flap angles $\beta_l$ and $\beta_t$. The control system is made up of several components including a passive mechanical network connected to the middle of the bridge deck with admittance functions $Y(s)$, a rack, three pinions with radius $r$, and a spring with spring constant $K_s$. The pinions are mounted in the inertial reference frame, and attached to the flaps. While this is not shown in Figure 4, the flaps are attached to remote hinges that are mounted on the bridge deck; these hinges are connected to the pinions in Figure 4 through addition mechanical equipment such as a cable arrangement. The pinions illustrated in Figure 4 are driven by a rack connected to the passive mechanical network $Y(s)$. The other end of the rack is connected to the spring $K_s$, which is anchored in the inertial reference framework. As is evident from Figure 4, the flaps are actuated by the controller $K(s)$ that consists of the mechanical network $Y(s)$, the rack, the spring $K_s$ and the pinions arrangement. Evidently the passive controller proposed here is insensitive to wind direction and requires no power supply.

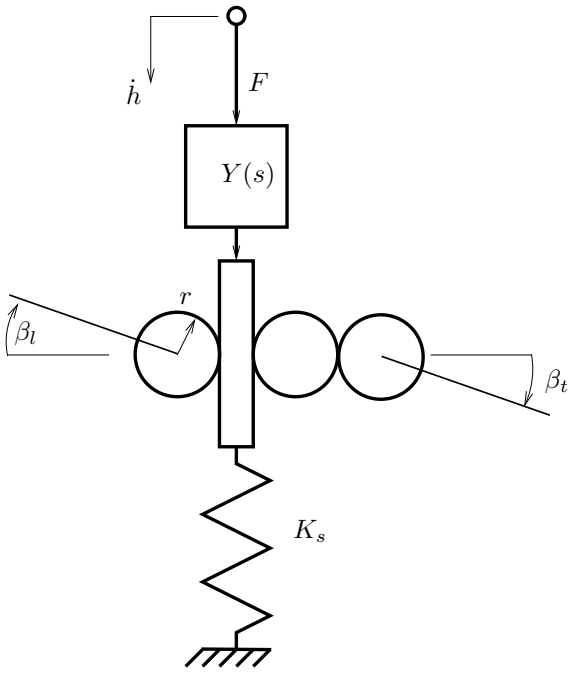


Fig. 4. Mechanical network used as compensator $K(s)$ in Fig. 3 for flap feedback control in which deck motion is used to control the bridge flaps.

The series connection of the admittances $Y(s)$ and $K_s$ is given by

$$\bar{K}(s) = \frac{K_s Y(s)}{K_s + sY(s)}. \quad (11)$$

The network through-variable associated with $\bar{K}(s)$ is the force $F(t)$, while the across-variable is the heave velocity $\dot{h}(t)$. Thus

$$F(s) \quad = \quad \bar{K}(s)\dot{h}(s). \quad (12)$$

The pinions rotate according as

$$r \times \beta = \frac{F}{K_s}, \quad (13)$$

where $\beta$ denotes both $\beta_l$ and $\beta_t$. From (11), (12) and (13), we have

$$K(s) = \frac{Y(s)}{rK_s + rsY(s)}, \quad (14)$$

which maps $\dot{h}$ into the flap angles.

The control system design will focus on the optimization of $K(s)$, which will be constrained to be passive and so:

$$\int_{-\infty}^{T} F(t)\dot{h}(t)dt \geq 0$$

for all terminal times $T$ [14]. The control system illustrated in Figure 4 is only one of many possible configurations.

Fig. 5 taken from [10] is the root-locus diagram for the open-loop system in which the wind speed $U$ is the varied parameter. There are two oscillatory structural (flutter) modes due to the heaving and pitching of the bridge deck. It is clear that the critical wind speeds for flutter and torsional divergence are around 52 m/s and 70 m/s, respectively.

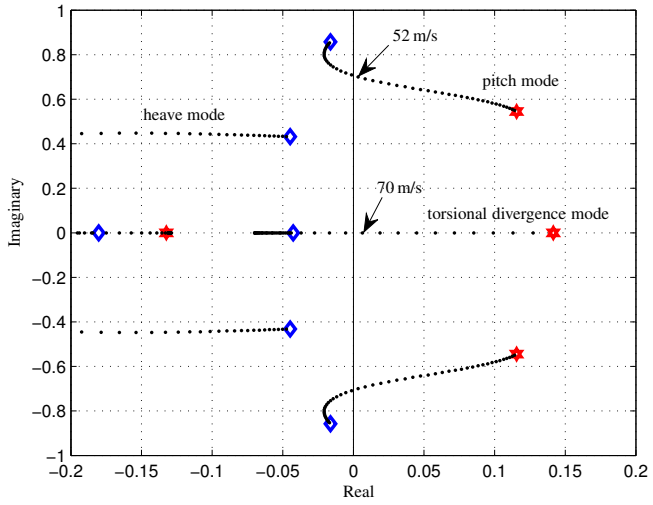


Fig. 5. Root-loci of the Akashi Kaikyo suspension bridge section. The wind speed is swept from 30 m/s to 80 m/s, with the low-speed ends of the root loci marked with (blue) diamonds and the high-speed ends marked with (red) hexagons. The pitch mode goes unstable at approximately 52 m/s, while the torsional divergence mode goes unstable at approximately 70 m/s.

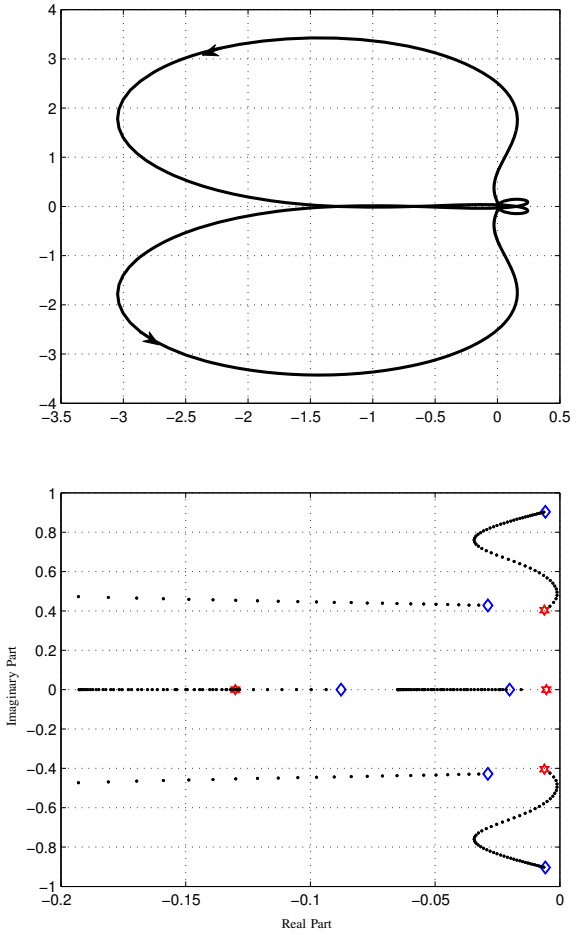


Fig. 6. The upper diagram shows the Nyquist diagram of the Akashi Kaikyo suspension bridge section at a wind speed of 65 m/s with $K(s) = 0.25$ and flap length 1.5 m. The lower diagram shows the root loci of the closed-loop system. The wind speed is swept from 14 m/s to 69 m/s, with the low-speed ends of the root loci marked with (blue) diamonds and the high-speed ends marked with (red) hexagons.

### B. Results

In this section we optimize the compensator $K(s)$ shown in Figure 3. For comparason purposes we begin by investigating the response characteristics for pure gain feedback. By setting $K(s) = 0.25$, with flap lengths 1.5 m, we obtain the Nyquist diagram (for the loop break point at $\Delta$ in Figure 3) and the associated closed-loop root loci in Figure 6. It is clear from this figure that the system is closed-loop stable with the critical flutter speed increased to 69 m/s, but with very poor robustness margins (see the region around the $-1$ point corresponding to 2 anti-clockwise encirclements).

We will now consider a dynamic compensator $K(s)$ that is designed to improve robustness at higher wind speeds. This is achieved using the design objective:

$$\min_{K(s)} \left\{ \max_{G_i(s,p)} \| \frac{1}{1 - G_i(s,p)} \|_\infty \right\} \quad i = 1, \ldots n. \qquad (15)$$

in which $\| \cdot \|_\infty$ is the frequency-response infinity norm [9]. The aim of this performance criterion is to maximise the distance between the compensated Nyquist diagram and the -1 point, with the correct winding number, thereby maximizing the closed-loop robust stability margin relative to additive-type perturbations [9]. Each of the transfer functions $G_i(s,p)$ correspond to the break point $\Delta$ in Fig. 3, and are a function of the Laplace variable $s$ and the optimization variables $p$ that include the parameters of the passive mechanical network $Y(s)$, the spring stiffness $K_s$, pinions radius $r$ and the flap chords. For the purpose of solving the optimization problem $n$ discrete wind speeds $U_i$ are used; this leads to the indexing $G_i(s,p)$. It is noted that maximizing the distance between the Nyquist diagram and the -1 point, for all frequencies, is equivalent to minimizing $\| \frac{1}{1-G_i(s,p)} \|_\infty$ [9]. In other words, the index (15) requires the distance between the Nyquist diagram and the -1 point to be maximized across all frequencies for the worst-case wind speed.

To ensure that the optimization problem is properly posed

a number of constraints must be put in place that operate in conjunction with (15).

1) The closed-loop eigenvalues are constrained to have negative real parts to ensure stability. This is equivalent to ensuring that the Nyquist plot encircles the -1 point the correct number of times. For wind speed above the critical flutter speed, but below the critical torsional divergence speed, a winding number of $N = 2$ is required.
2) The leading- and trailing-edge flap chords are assumed to have the same length. Since they are design parameters, they must be constrained to be non-negative and below some maximum; ($\leq$2 m is used in the studies presented here).
3) The Y(s) in Fig. 4 will be constrained to be passive so that they can be synthesized using only passive mechanical components (springs, dampers and inerters) [14]. This is ensured by imposing a positive-reality constraint on its coefficients [15]. If $Y(s)$ is passive, $K(s)$ in Figs. 4 and 3 is passive.

The resulting nonlinear constrained optimization problem is solved using MATLAB's sequential quadratic programming algorithm FMINCON.

### C. First-order Compensator

In the first design study we consider $Y(s)$ has the following first-order transfer function:

$$Y(s) = Y\frac{s+z_0}{s+p_0} \tag{16}$$

in the control loop in Figs. 3 and 4. Here both flaps have the same length $\leq 2$, and $z_0$ and $p_0$ are constrained to be non-negative to ensure passivity. The compensator $K(s)$ can be easily derived by equation (14). The wind speeds considered in the optimization process are 14 m/s to 69 m/s in steps of 5 m/s. The result of the optimization calculation is

$$\begin{aligned} Y = 0.1899, z_0 = 0.6810, p_0 = 0.0666, \\ K_s = 1.1827\,N/m, r = 1.0521. \end{aligned} \tag{17}$$

with both optimal flap chords 0.5100 m. It's clear that $Y(s)$ is a lag network, which can be realized using springs and dampers only. Figure 7 shows the compensated ($K(s)$ given by (14), (16) with values in (17)) Nyquist diagrams for the loop break point at $\Delta$ in Figure 3, and the associated closed-loop root loci.

It is clear from these diagrams that the system is closed-loop stable with the critical flutter speed increased to $69\,m/s$. By comparing the Nyquist diagrams in Figures 7 and 6, it is clear that the phase compensation introduced by (14), (16) and (17) has 'opened up' the N=2 region significantly, and thus greatly improved robustness margins have been obtained. The lower root locus diagram shows that the flutter (heave and pitch) modes are well damped at U=69 m/s. In this case the index given in (15) had a value of 1.2738 indicating that the smallest distance, across all frequencies, to the -1 point, is 0.7851. This distance can be interpreted as a robustness margin.

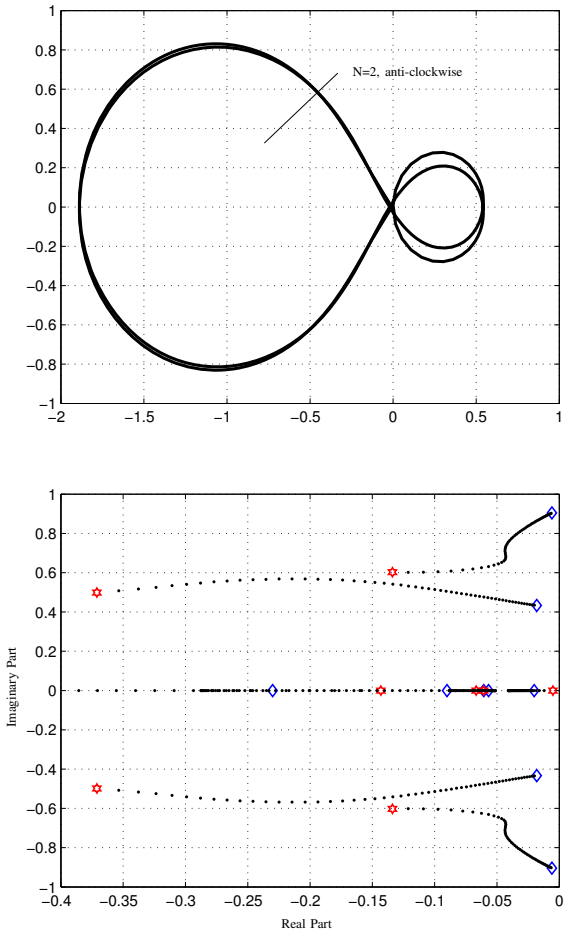


Fig. 7. The upper diagram shows the compensated Nyquist diagram of the Akashi Kaikyo suspension bridge section at a wind speed of 65 m/s with compensator $K(s)$ given by (14), (16) with parameters in (17). The lower diagram shows the root loci of the compensated closed-loop system. The wind speed is swept from 14 m/s to 69 m/s, with the low-speed ends of the root loci marked with (blue) diamonds and the high-speed ends marked with (red) hexagons.

### D. Second-order Compensator

Now we consider $Y(s)$ has the following second-order transfer function:

$$Y(s) = \frac{a_2 s^2 + a_1 s + a_0}{s^2 + d_1 s + d_0} \tag{18}$$

in the control loop in Figs. 3 and 4 with the coefficients constrained to ensure that $K(s)$ is positive-real [16]. Positive reality requires each of the five coefficients in (18) to be non-negative together with the condition $a_1 d_1 \geq \left(\sqrt{a_0} - \sqrt{d_0 a_2}\right)^2$; see Theorem 2 in [15]. The wind speeds considered in the optimization process are 14 m/s to 69 m/s in steps of 5 m/s. When the coefficients in (18) are optimized, the following numerical values were obtained

$$\begin{aligned} a_2 = 0.6119,\, a_1 = 1.4059, a_0 = 1.1225, d_1 = 9.0054, \\ d_0 = 0.7331, K_s = 2.0115\,N/m, r = 0.4969. \end{aligned} \tag{19}$$

with both flap chords set at 0.5000 m.

The compensated ($K(s)$ given by (14), (18) with optimized parameters in (19)) Nyquist diagram for the loop break point $\Delta$ in Fig. 3, and the associated closed-loop root loci are shown in Fig. 8. From the Nyquist plots in Figures 8 and 7,

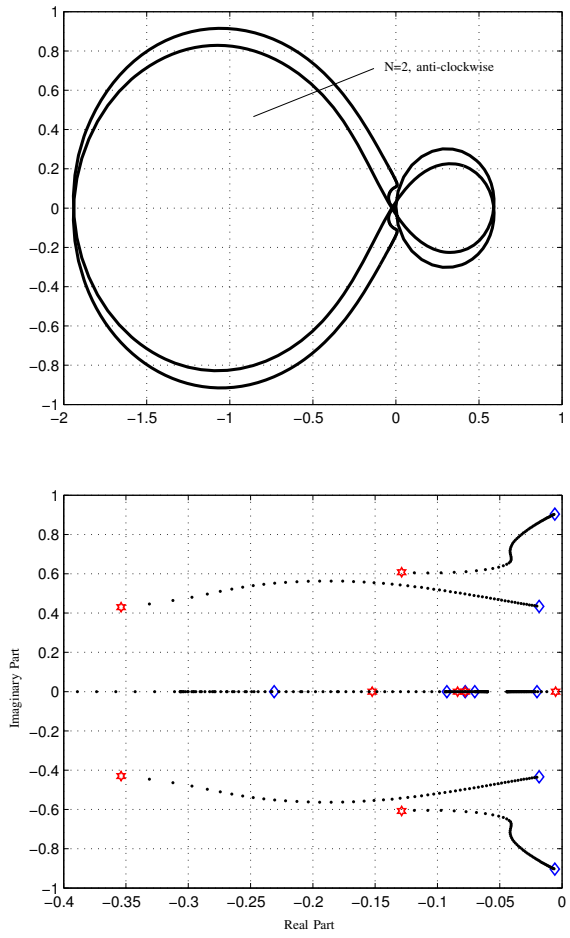


Fig. 8. The top diagram shows the compensated Nyquist diagram of the Akashi Kaikyo suspension bridge section at a wind speed of 65 m/s with compensator $K(s)$ given by (14), (18) with parameters in (19). The lower diagram shows the root loci of the compensated closed-loop system. The wind speed is swept from 14 m/s to 69 m/s, with the low-speed ends of the root loci marked with (blue) diamonds and the high-speed ends marked with (red) hexagons.

it is clear that very little improvement is achieved using a second-order $Y(s)$ as compared with a first-order network $Y(s)$ in terms of robustness. The root locus diagram shows that the flutter modes are well damped at U=69 m/s. In this case the index given in (15) had a value of 1.2717 indicating that the smallest distance, across all frequencies, to the -1 point, is 0.7863 that is only a marginal improvement over the first-order case (0.7851).

## IV. Conclusions

This paper addresses the problem of stabilizing flutter instabilities in long-span suspension bridges by employing controllable leading- and trailing-edge flaps. Our results show that passive heave velocity feedback can be used to increase the critical wind speed for flutter with improved robustness characteristics. This paper also removes the wind direction dependence of the control system given in [2], which uses deck pitch angle feedback. Insensitivity to the wind direction is achieved using identical flaps driven by the same passive heave velocity (of the deck) driven compensator. It is noted that the compensator presented here is ineffective in increasing the critical wind speed for torsional divergence (because the flap arrangement produces a low net moment on the deck), but in many cases this is already above that of any wind likely to be encountered.

## References


[1] K. Y. Billah and R. H. Scanlan, "Resonance, tacoma narrows bridge failure, and undergraduate physics textbooks," *American Journal of Physics*, vol. 59, no. 2, pp. 118–124, 1991.

[2] J. M. R. Graham, D. J. N. Limebeer, and X. Zhao, "Aeroelastic control of long-span suspension bridges," *Journal of Applied Mechanics*, vol. 78, pp. 041 018–1 to 041 018–12, 2011.

[3] T. Theodorsen, "General theory of aerodynamic instability and the mechanisms of flutter," *NACA Report, TR-496*, 1934.

[4] P. Omenzetter, K. Wilde, and Y. Fujino, "Suppression of wind-induced instabilities of a long span bridge by a passive deck-flaps control system part I: Formulation," *Journal of Wind Engineering*, vol. 87, pp. 61–79, 2000.

[5] ——, "Suppression of wind-induced instabilities of a long span bridge by a passive deck-flaps control system part II: Numerical simulations," *Journal of Wind Engineering*, vol. 87, pp. 81–91, 2000.

[6] D. C. del Arco and A. C. Aparicio, "Improving suspension bridge wind stability with aerodynamic appendages," *Journal of Structural Engineering*, vol. 125, no. 12, pp. 1367–1375, 1999.

[7] H. I. Hansen and P. Thoft-Christensen, "Active flap control of long suspension bridges," *Journal of Structural Control*, vol. 8, no. 1, pp. 33–82, 2001.

[8] K. Wilde and Y. Fujino, "Variable-gain control applied to aerodynamic control of bridge deck flutter." Proceedings of 35th Conference on Decision and Control, Kobe, Japan, 1996, pp. 682–687.

[9] M. Green and D. J. N. Limebeer, *Linear Robust Control*. Englewood Cliffs, New Jersey 07632: Prentice Hall, 1995.

[10] J. M. R. Graham, D. J. N. Limebeer, and X. Zhao, "Aeroelastic moldelling of long-span suspension bridges." Proceedings of the 18th IFAC World Congress, Milano, Italy, August 2011, pp. 9212–9217.

[11] R. L. Bisplinghoff, H. Ashley, and R. L. Halfman, *Aeroelasticity*. Addison-Wesley, 1955.

[12] W. R. Sears, "Operational methods in the theory of airfoils in non-uniform motion," *Journal of the Franklin Institute*, vol. 230, pp. 95–111, 1940.

[13] D. A. Peters, "Two-dimensional incompressible unsteady airfoil theory — an overview," *Journal of Fluids and Structures*, vol. 24, pp. 295–312, 2008.

[14] M. C. Smith, "Synthesis of mechanical networks: The inerter," *IEEE Trans. Automatic Control*, vol. 47, no. 10, pp. 1648–1662, October 2002.

[15] S. Evangelou, D. J. N. Limebeer, R. S. Sharp, and M. C. Smith, "Steering compensators for high-performance motorcycles," *ASME J. Applied Mechanics*, vol. 74, no. 5, pp. 332–346, 2007.

[16] R. W. Newcomb, *Linear Multiport Synthesis*. McGraw-Hill, New York, 1966.